PHYSICAL REVIEW E **76**, 036406 (2007)

Wave packet simulation of dense hydrogen

B. Jakob, P.-G. Reinhard, C. Toepffer, and G. Zwicknagel
Institut für Theoretische Physik II, Universität Erlangen-Nürnberg, Staudtstrasse 7, D-91058 Erlangen, Germany

(Received 15 February 2007; revised manuscript received 31 May 2007; published 26 September 2007)

Dense hydrogen is studied in the framework of wave packet molecular dynamics. In this semiquantal many-body simulation method the electrons are represented by wave packets which are suitably parametrized. The equilibrium properties and time evolution of the system are obtained with the help of a variational principle. At room temperature the results for the isotherms are in good agreement with anvil experiments. At higher densities beyond the range of the experimental data a transition from a molecular to a metallic state is predicted. The wave packets become delocalized and the electrical conductivity increases sharply. The phase diagram is calculated in a wide range of the pressure-density-temperature space. The observed transition from the molecular to metallic state is accompanied by an increase in density in agreement with recent reverberating shock wave experiments.

DOI: 10.1103/PhysRevE.76.036406 PACS number(s): 52.65.Yy, 02.70.Ns, 05.70.Ce, 62.50.+p

I. INTRODUCTION

Although hydrogen is the simplest of all chemical elements, its physical properties under extreme conditions are still not well known, neither experimentally nor theoretically. As hydrogen diffuses strongly into other materials, static anvil experiments can only be done at rather low temperatures [1]. A transition to a metallic phase has been predicted by extrapolation of experimental results [2]. Complementary shock wave experiments show direct evidence for such a transition [3]. However, the strong compression observed in the earlier measurements with the Nova Laser [4,5] has not been confirmed in more recent experiments with the *Z* machine [6–8] or with explosives [9,10].

The equation of state of hydrogen and hydrogen-rich mixtures determines the structure of brown dwarfs and large gas planets [11–14]. Also for the production of energy by inertial fusion in pellets the behavior of deuterium under extreme conditions of temperature and pressure must be known [16,17].

Although the Coulomb interaction between the constituents has been known for more than two centuries, the hydrogen phase diagram still constitutes a great challenge to many-body physics. The possibility of a metallization at high densities was discussed already in 1935 by Wigner and Huntington [18]. Since then the physical properties of dense hydrogen have been studied with a variety of methods. On one hand, there is the chemical picture [19,20], where one considers a system consisting of the components H_2, H, protons, electrons, and possibly others, and minimizes the free energy [12,21,22]. This requires effective interactions, pair correlations, exchange parts, and polarization corrections as input [23]. In contrast, the *ab initio* methods start on a more fundamental level, but approximations are necessary for practical solutions. Often only the electrons are treated quantum mechanically, while the nuclei are supposed to move classically because of their large mass. In tight-binding molecular dynamics (TBMD) the forces on the nuclei are obtained from the total energy of bound electrons whose wave functions are parametrized to fit, e.g., the H_2 molecule and other suitable data [24]. Alternatively, the electron energy is calculated in the local density approximation (LDA) of the density functional theory (DFT). Either the Kohn-Sham equations are diagonalized directly [25] or the Kohn-Sham functional is minimized [26–29]. In more recent work the generalized gradient approximation (GGA) is used for the exchange and correlation energies, see, e.g., Refs. [14,15,30–34]. As long as the underlying density functionals are independent of the temperature, this density functional molecular dynamics (DFMD) is valid, i.e., at low temperatures. In the variational density matrix (VDM) method the elements of the density matrix are parametrized, e.g., by Gaussians, and the parameters are determined variationally [35]. Alternatively the density is calculated by a Monte Carlo evaluation of a path integral (PIMC). As this requires a sum over all permutations of single particles, there arises a sign problem for electrons. The paths must be restricted in order to avoid the crossing of nodes (RPIMC). For that purpose either the nodes of the free particle density matrix are employed [36] or those of the VDM [37]. So RPIMC is rather a high-temperature method. In the recently reformulated direct path integral Monte Carlo method (DPIMC) the exchange problem is contained in a Slater determinant which can be calculated by stable algebraic methods [38,39]. However, convergence problems have been reported for the DPIMC at low temperatures when the formation of bound states becomes important [40].

In this paper, we investigate the metallization of hydrogen using wave packet molecular dynamics (WPMD) simulations. In this method, the electron wave functions are parametrized in terms of moving Gaussians with variable width. Appropriate equations for equilibrium and dynamic properties of the system are obtained with the help of a variational principle. The WPMD approach has been successful in the description of many-body dynamics such as the scattering of composite systems such as atoms and molecules [41] and of heavy ions [42,43]. As in other methods the fermion problem imposes a major challenge. In earlier applications of WPMD to dense matter [44–49] various compromises were made in this respect, for example, the electrons were only antisymmetrized pairwise or the antisymmetrization was neglected in the matrix elements of the electron-electron interaction. Such simplifications had limited the regime of application. The present results are obtained with an improved WPMD in which antisymmetrization is fully implemented which allows one to proceed more deeply into the regime of dense hydrogen. In Sec. II we describe the WPMD as it is used in this study. For test purposes, the method is applied to model systems in Sec. III. Isothermal and isochoric changes, the conductivity and the resulting phase diagram of hydrogen are discussed in Sec. IV. Our conclusions are presented in Sec. V.

II. WAVE PACKET MOLECULAR DYNAMICS (WPMD)

A. Quasi-classical equations of motion

We consider a wave function Ψ for N particles which is parametrized by M time-dependent parameters $\{v_i(t)|i=1,\ldots,M\}$

$$\Psi(t)=\Psi[v_1(t),\ v_2(t),\ldots,\ v_M(t)] \tag{1}$$

with the normalization $\langle\Psi(t)|\Psi(t)\rangle=1$ for all times t. The dynamics, i.e., the time evolution of the $v_i(t)$ can be obtained from the time-dependent variational principle by minimizing the action $\int\mathcal{L}[\Psi,\Psi^*]dt$ with the Lagrangian

$$\mathcal{L}[\Psi,\Psi^*]=\langle\Psi(t)|i\hbar\frac{\partial}{\partial t}-\hat{H}|\Psi(t)\rangle. \tag{2}$$

Introducing the expectation value

$$\mathcal{H}\{v\}=\langle\Psi|\hat{H}|\Psi\rangle \tag{3}$$

and the norm matrix $\mathcal{N}$ with the elements

$$\mathcal{N}_{ij}=-2\hbar\,\mathrm{Im}\left\langle\frac{\partial}{\partial v_i}\Psi\Big|\frac{\partial}{\partial v_j}\Psi\right\rangle \tag{4}$$

the Euler-Lagrange equations yield

$$0=\frac{\mathrm{d}}{\mathrm{d}t}\frac{\partial\mathcal{L}}{\partial\dot{v}_i}-\frac{\partial\mathcal{L}}{\partial v_i}=\sum_{j=1}^{M}\mathcal{N}_{ij}\dot{v}_j-\frac{\partial\mathcal{H}}{\partial v_i}. \tag{5}$$

If the norm matrix can be inverted the equations of motion

$$\dot{v}_i=\sum_{j=1}^{M}(\mathcal{N}^{-1})_{ij}\frac{\partial\mathcal{H}}{\partial v_j} \tag{6}$$

yield an approximate solution in a Hilbert space which is restricted by the parametrization prescribed through Eq. (1).

Equations (6) resemble Hamiltonian equations except for the norm matrix $\mathcal{N}^{-1}$. At a given point in parameter space and assuming M to be even, one can conceive a transformation

$$d\mathbf{k}=\mathcal{B}d\mathbf{v},\quad \mathcal{B}\mathcal{N}^{-1}\mathcal{B}=\begin{pmatrix}0 & \mathbb{1}\\ -\mathbb{1} & 0\end{pmatrix} \tag{7}$$

to M canonical coordinates $\mathbf{k}$ for which the equations of motion

$$\dot{k}_i=\sum_{j=1}^{M}\begin{pmatrix}0 & \mathbb{1}\\ -\mathbb{1} & 0\end{pmatrix}_{ij}\frac{\partial\mathcal{H}\{k\}}{\partial k_j} \tag{8}$$

are symplectic. This transformation will be used in the next section for deriving a compact formula for ensemble averages.

B. Time average and ensemble average

For equilibrium expectation values, the equations of motion (6) need not be solved explicitly, but can be replaced by an ensemble average with appropriate statistical weight [50]. Consider a canonical ensemble at a temperature $T=(k_B\beta)^{-1}$ and coordinates $\{k(t)\}=\{k_1(t),\ k_2(t),\ldots,\ k_M(t)\}$ with symplectic equations of motion (8). Then the ensemble expectation value of a dynamical observable A is

$$\bar{A}=\frac{1}{Z}\int d^Mk e^{-\beta\mathcal{H}\{k\}}A\{k\}, \tag{9a}$$

$$Z=\int d^Mk e^{-\beta\mathcal{H}\{k\}}. \tag{9b}$$

The nonsymplectic equations of motion (6) are related to symplectic ones through the transformation (7) which is described by a matrix $\mathcal{B}$. Then the volume elements are related by

$$d^Mk=|\det\mathcal{B}|d^Mv,\quad |\det\mathcal{B}|=(\det\mathcal{N})^{1/2}.$$

This allows us to reformulate the ensemble expectation value (9a) and (9b) in terms of the coordinates $\{v_i\}$ as

$$\bar{A}=\frac{1}{Z}\int d^Mv(\det\mathcal{N})^{1/2}e^{-\beta\mathcal{H}\{v\}}A\{v\}, \tag{10a}$$

$$Z=\int d^Mv(\det\mathcal{N})^{1/2}e^{-\beta\mathcal{H}\{v\}}. \tag{10b}$$

We will evaluate in the following all expectation values according to that expression using properly weighted Monte Carlo sampling of the integrals [50].

C. Wave-packet ansatz

The constituents of the hydrogen systems are protons and electrons. The protons are treated classically using simply their positions as dynamical degrees of freedom. The electrons require a quantum mechanical description which we will realize by a variational ansatz in terms of Gaussian wave packets. The necessarily finite number $k=1,\ldots,\ N$ of electrons and protons is placed in a cubic simulation box of length L. The bulk system is simulated by copying the simulation box periodically in all three directions which produces a bcc lattice of boxes. The lattice states $\varphi_{k,\vec{q}}$ are composed from periodic copies of Gaussian packets

$$\varphi_{k,\vec{q}}(\vec{x})=\exp\left(i\frac{2\pi\vec{q}}{L}\cdot\vec{x}\right)\sum_{\vec{n}\in\mathbb{Z}^3}\xi_k(\vec{x}-\vec{n}L),\quad k=1,\ldots,\ N, \tag{11a}$$

$$\xi_k(\vec{x}) = \left(\frac{3}{2\pi\gamma_k^2}\right)^{3/4} \exp\left[-\left(\frac{3}{4\gamma_k^2} - \frac{ip_{\gamma,k}}{2\hbar\gamma_k}\right)(\vec{x}-\vec{r}_k)^2 + i\frac{\vec{p}_k}{\hbar}\cdot(\vec{x}-\vec{r}_k)\right]\chi_{\sigma_k}, \tag{11b}$$

modulated by a Bloch momentum $2\pi\vec{q}/L$ which is confined to the first Brillouin zone $\mathbb{Q}$ of the cubic lattice, i.e.,

$$\mathbb{Q} = \left\{ \vec{q} \middle| q_x, q_y, q_z \in \left]-\frac{1}{2}, +\frac{1}{2}\right]\right\}. \tag{12}$$

The wave packets ξ_k (11b), where χ_{σ_k} is a Pauli spinor, are tuned by the eight variational parameters

$$\{v_k(t)\} \equiv \{\vec{r}_k(t), \gamma_k(t), \vec{p}_k(t), p_{\gamma,k}(t)\}. \tag{13}$$

The wave functions (11a) look very similar to a Bloch wave. However, they involve an approximation: we neglect the **q** dependence of the model parameter v_k and let them depend only on k. This simplifies the calculations enormously.

The total many-body wave function is thought to be composed as a Slater determinant. Its handling, however, becomes impractical for a continuum of occupied single particle states as we encounter here. Thus we compute the energies directly from expressions which hold for independent and orthonormalized fermion states [51], namely,

$$E_{\text{kin}} = \sum_{k=1}^{N} \int_{\mathbb{Q}} d^3q (\tilde{\varphi}_{k,\vec{q}}|\hat{T}|\tilde{\varphi}_{k,\vec{q}}), \tag{14a}$$

$$E_{\text{pot}} = \sum_{k,k'=1}^{N} \int_{\mathbb{Q}} d^3q d^3q' [(\tilde{\varphi}_{k,\vec{q}}\tilde{\varphi}_{k',\vec{q}'}|\hat{V}|\tilde{\varphi}_{k,\vec{q}}\tilde{\varphi}_{k',\vec{q}'}) - (\tilde{\varphi}_{k,\vec{q}}\tilde{\varphi}_{k',\vec{q}'}|\hat{V}|\tilde{\varphi}_{k',\vec{q}'}\tilde{\varphi}_{k,\vec{q}})], \tag{14b}$$

$$(\tilde{\varphi}_{k,\vec{q}}|\tilde{\varphi}'_{k',\vec{q}}) = \delta_{kk'}\delta^3(\vec{q}-\vec{q}'). \tag{14c}$$

However, the Gaussian basis states (11a) and (11b) are nonorthogonal with the overlaps

$$\langle\varphi_{k,\vec{q}}|\varphi_{l,\vec{q}'}\rangle = (\mathbf{O})_{kl}\delta^3(\vec{q}-\vec{q}'). \tag{15a}$$

We formally orthonormalize that basis to

$$|\tilde{\varphi}) = \mathbf{Y}^{1/2}|\varphi\rangle, \quad \mathbf{Y} = \mathbf{O}^{-1}, \tag{16}$$

and insert that into the energies (14a)–(14c). This yields the expressions detailed in the next section.

D. Evaluation of energy

The Hamiltonian of the hydrogen system is given by

$$\hat{H} = \sum_{I=1}^{N} \frac{\hat{\vec{P}}_I^2}{2M} + \sum_{i=1}^{N} \frac{\hat{\vec{p}}_i^2}{2m} + \frac{e^2}{4\pi\varepsilon_0}\left(\sum_{I<J=1}^{N} \frac{1}{|\vec{R}_I - \vec{R}_J|} + \sum_{i<j=1}^{N} \frac{1}{|\vec{x}_i - \vec{x}_j|} - \sum_{I,j=1}^{N} \frac{1}{|\vec{R}_I - \vec{x}_j|}\right). \tag{17}$$

The most involved part is the energy expectation value for the quantum-mechanical electron system. For its evaluation, it is advantageous to write the wave function (11a) as a Fourier series

$$\varphi_{k,\vec{q}}(\vec{x}) = \sum_{\vec{\nu}\in\mathbb{Z}^3} w_{\vec{\nu}}^k \exp\left(i\frac{2\pi(\vec{\nu}+\vec{q})}{L}\cdot\vec{x}\right),$$

$$w_{\vec{\nu}}^k = \frac{1}{L^3}\int \frac{d^3x}{(2\pi)^3} \exp\left(-i\frac{2\pi\vec{\nu}}{L}\cdot\vec{x}\right)\xi_k(\vec{x}), \tag{18}$$

where the Fourier coefficient $w_{\vec{\nu}}^k$ is a spinor.

A first key quantity is the overlap **O** between the single particle wave functions which becomes

$$(\mathbf{O})_{kl} = \langle\varphi_k|\varphi_l\rangle = L^3 \sum_{\vec{\mu}\in\mathbb{Z}^3} (w_{\vec{\mu}}^k)^* w_{\vec{\mu}}^l, \tag{19a}$$

where $|\varphi_l\rangle \equiv |\varphi_{l,\vec{q}=0}\rangle$ has been used as an abbreviation. In a similar fashion, we find for the overlap matrix elements of the electron kinetic energy

$$(\mathbf{T})_{kl} = \langle\varphi_k|\frac{\hat{\vec{p}}^2}{2m}|\varphi_l\rangle = \frac{2\hbar^2\pi^2 L}{m}\sum_{\vec{\mu}\in\mathbb{Z}^3} \vec{\mu}^2 (w_{\vec{\mu}}^k)^* w_{\vec{\mu}}^l. \tag{20}$$

Both together allow us to compose the kinetic energy of the approximate Bloch ansatz (11a) as

$$E_{\text{kin}}^{(\text{BL})} = \frac{\hbar^2\pi^2}{2mL^2}N + \text{Tr}(\mathbf{T}\cdot\mathbf{Y}). \tag{21a}$$

The evaluation of the various terms of Coulomb energy requires a generalized "overlap" where the Fourier components are shifted relative to each other by a vector $\vec{\nu}$. It reads

$$(\mathbf{D}_{\vec{\nu}})_{kl} = \sum_{\vec{\mu}\in\mathbb{Z}^3} (w_{\vec{\mu}}^k)^* w_{\vec{\mu}+\vec{\nu}}^l. \tag{22}$$

Then the quantum-mechanical energies can be written as

$$E_{\text{qm}} = E_{\text{kin}} + E_{\text{pot}}^{ep} + E_{\text{pot}}^{ee}, \tag{23a}$$

$$E_{\text{pot}}^{ep} = -\frac{e^2}{4\pi\epsilon_0}\frac{L^2}{2\pi}\sum_{\vec{\nu}\in\mathbb{Z}^3\setminus\{0\}} \frac{1}{\vec{\nu}^2}\text{Tr}(\mathbf{D}_{\vec{\nu}}\cdot\mathbf{Y})\sum_{J=1}^{N}\exp\left(i\frac{2\pi\vec{\nu}}{L}\cdot\vec{R}_J\right), \tag{23b}$$

$$E_{\text{pot}}^{ee} = \frac{e^2}{4\pi\epsilon_0}\frac{L^5}{2\pi}\left(\sum_{\vec{\nu}\in\mathbb{Z}^3\setminus\{0\}} \frac{1}{\vec{\nu}^2}\text{Tr}(\mathbf{D}_{-\vec{\nu}}\cdot\mathbf{Y})\text{Tr}(\mathbf{D}_{\vec{\nu}}\cdot\mathbf{Y}) - \sum_{\vec{\nu}\in\mathbb{Z}^3} I_{\vec{\nu}}\text{Tr}(\mathbf{D}_{-\vec{\nu}}\cdot\mathbf{Y}\cdot\mathbf{D}_{\vec{\nu}}\cdot\mathbf{Y})\right), \tag{23c}$$

$$I_{\vec{\nu}} = \int_{-\infty}^{\infty} \frac{d^3r L^4}{\pi^4|\vec{r}|r_x^2 r_y^2 r_z^2}\sin^2\left(\frac{\pi r_x}{L}\right)\sin^2\left(\frac{\pi r_y}{L}\right)\sin^2\left(\frac{\pi r_z}{L}\right) \times\exp\left(i\frac{2\pi\vec{\nu}}{L}\cdot\vec{r}\right), \tag{23d}$$

where E_{kin} stands for the kinetic energy of the electrons, E_{pot}^{ep} for the electron-proton interaction, and E_{pot}^{ee} for direct and

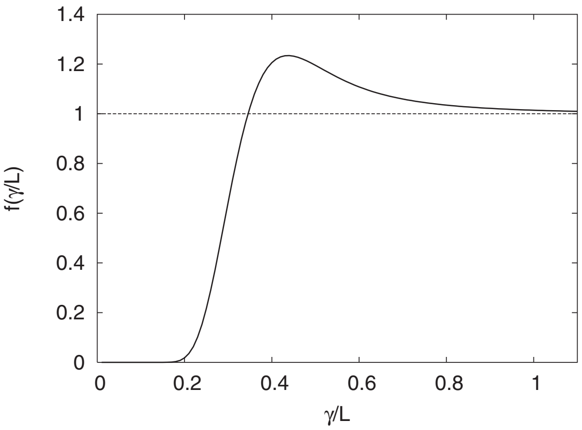

FIG. 1. The function $f(\gamma/L)$ for the tight binding energy (25). The dashed line at value 1 indicates the relative position of the kinetic energy (21a) from the Bloch ansatz.

exchange terms of the Coulomb interaction of electrons. Note that the exchange term vanishes for electrons with opposite spin direction. The inverse overlap matrix $\mathbf{Y}$ accounts for antisymmetrization. The integral $I_{\vec{\nu}}$ which occurs in the exchange contribution is finite for $\vec{\nu}=0$ and behaves $\propto \nu^{-2}$ for $\nu \gg 1$. The fermion sign problem does not appear in that energy and the whole computations have been reduced to stable matrix operations at a tolerable numerical expense $O(N^3)$.

The kinetic energy E_{kin} is not yet finally defined. The result (21a) obtained from the approximate Bloch ansatz (11a) and (18) contains a constant grid energy $\hbar^2\pi^2/(2mL^2)$ per particle. We will show in Sec. III that this term is both necessary and sufficient to give the correct energy for delocalized electrons in jellium. However, for localized and almost nonoverlapping electron wave functions a tight binding approximation is more appropriate:

$$\varphi_{k,\vec{q}}^{(\text{TB})}(\vec{x}) = \sum_{n \in \mathbb{Z}^3} \exp(i2\pi\vec{q}\cdot\vec{n})\xi_k(\vec{x}-\vec{n}L). \tag{24}$$

In that ansatz, each packet ξ_k contributes with a constant phase factor. The Fourier coefficients then depend on $\vec{q}$. Nevertheless, the kinetic energy of an electron with $\vec{p}=0, p_\gamma=0$ per box can still be calculated in a straightforward manner. The result is

$$E_{\text{kin}}^{(\text{TB})} = \frac{\hbar^2\pi^2}{2mL^2} f\left(\frac{\gamma}{L}\right) + \text{Tr}(\mathbf{T}\cdot\mathbf{Y}), \tag{25}$$

where the ratio of width γ and box size L obviously regulates the regime. The function $f(\gamma/L)$ is shown in Fig. 1. As expected it approaches the values 1 for $\gamma \geq L$ and 0 for $\gamma \leq L$. The regime of small widths $\gamma < 0.35L$ has $f < 1$ and thus the tight-binding ansatz becomes favorable whereas $f > 1$ in the regime of large widths makes the approximate Bloch ansatz preferable. Instead of searching for an optimal superposition of Eqs. (11a) and (24) by variation, we minimize the kinetic energy *ad hoc* by choosing the minimum of the switch factors. This yields the kinetic energy finally as

$$E_{\text{kin}} = \frac{\hbar^2\pi^2}{2mL^2}\sum_k \tilde{f}\left(\frac{\gamma_k}{L}\right) + \text{Tr}(\mathbf{T}\cdot\mathbf{Y}), \tag{26a}$$

$$\tilde{f}\left(\frac{\gamma}{L}\right) = \min\left\{f\left(\frac{\gamma}{L}\right),\ 1\right\}. \tag{26b}$$

This is the form to be used in the total energy (23a)–(23d).

The protons are treated classically with the help of the Ewald technique [52]. The expectation values (10b) are calculated by Monte Carlo (MC) simulations with the Metropolis algorithm [50], the dynamic simulations are performed by solving the equations of motion (6) with a Runge-Kutta time integration scheme of second order (midpoint method), see, e.g., Ref. [53], which we preferred here instead of the more frequently used fourth and fifth order Runge-Kutta schemes. Details of the numerical implementation can be found in [54,55].

E. Evaluation of pressure *P*

The key observable in most measurements is the pressure P. From the theoretical side, it can be expressed with the help of the virial theorem [56]

$$P = \frac{n}{3}\left(2\frac{\langle E_{\text{kin}}\rangle}{N} + \frac{\langle E_{\text{pot}}\rangle}{N}\right) \tag{27}$$

through the expectation values of the kinetic and potential energy of both electrons and protons. That expression is formally simple. It is, however, a very sensitive quantity in practice as it depends crucially on a subtle balance between kinetic and potential energy.

III. FREE ELECTRON GAS AND ONE-COMPONENT PLASMA (OCP)

For a test of the WPMD, we compare with the exactly known Hartree-Fock (HF) solution for the free electron gas and investigate a simple OCP model for metallic hydrogen. The HF ground-state energy of a dense polarized free electron gas, i.e., electrons and a homogeneous neutralizing background, is [51]

$$\frac{E^e}{N} = \left(\frac{1.105}{r_s^2} - \frac{0.458}{r_s}\right)E_h, \quad E_h = \frac{e^2}{4\pi\varepsilon_0 a_0}, \tag{28}$$

where $r_s=[3/(4\pi n)]^{1/3}/a_0$ is the density parameter of an electron gas with a number density n and $a_0=4\pi\varepsilon_0\hbar^2/me^2$ is the Bohr radius. The WPMD MC simulations were done at $T=30$ K, near the ground state. We first investigate the dependence of the total energy E_{tot} on the number of particles in the simulation box at a fixed density $n=2\times 10^{29}$ m^{-3}, see Fig. 2. Already the case of one single particle per box provides a reasonable agreement with the HF result. The wave packet is a plane wave with $\vec{p}\to 0$ and $\gamma\to\infty$ and the energy would vanish except for the Bloch term [first term in Eq. (21a)] which describes the interaction of the electron with its own copies. For a few particles in the box, the interaction limits the relative width γ/L and the agreement becomes worse. But for more than 27 electrons in the box, the total

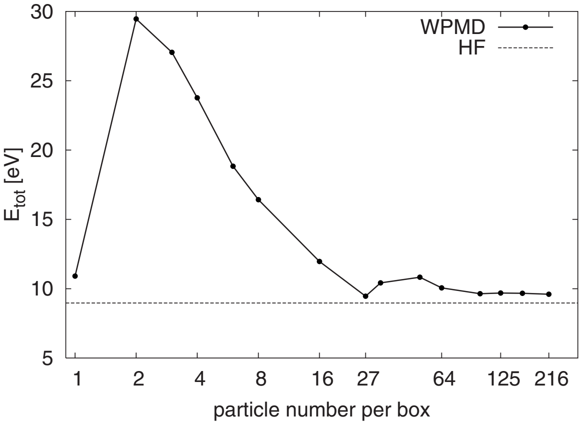

FIG. 2. The total energy of a polarized free electron gas at $n=2\times10^{29}$ m^{-3} as a function of the particle number in the simulation box.

energies agree again nicely with the HF values and for cubic numbers 27, 64, 125, 216,…, a cubic lattice is formed.

A one-component plasma (OCP) model for metallic hydrogen at low temperatures can be obtained by superimposing a homogeneous unpolarized electron gas with protons. The kinetic energy of the OCP at $T=0$ is zero and the potential energy of the protons in a homogeneous electron background is [57]

$$\frac{E^{\mathrm{OCP}}}{N} = -\frac{0.899}{r_s}E_h. \tag{29}$$

The total energy of electrons and protons becomes

$$\frac{E^{e+\mathrm{OCP}}}{N} = \left(\frac{1.105}{r_s^2} - \frac{1.357}{r_s}\right)E_h. \tag{30}$$

The first term represents the kinetic energy and the second the potential energy. This assignment allows one to compute the pressure easily with Eq. (27). The solid line in Fig. 3 shows the pressure as a function of the density. The overall trends look realistic. However, at low densities near $n=2\times10^{29}$ m^{-3}, the e+OCP pressure becomes negative. This indicates an instability. At these low densities the electrons become localized and bound states are formed. But this cannot be described with this simple e+OCP model. Because of the strong coupling, more refined temperature-dependent expressions for E^{OCP} [58] yield for 300 K results which hardly differ from those of Eq. (29) on the scale of Fig. 3.

Figure 3 also shows the results from two WPMD simulations at low temperature ($T=300$ K) with different numbers of electrons per simulation box. The numerical simulation provides positive pressure everywhere. As shown below there is a transition to molecular bound electron states at low densities. For high densities, the results agree with the simple OCP model. The convergence with respect to the particle number depends on the regime. Good convergence with 128 electrons is achieved at low and moderate densities while more particles are required at higher densities.

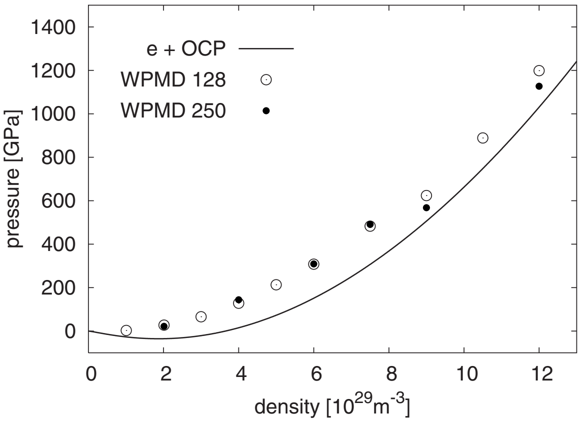

FIG. 3. Pressure of hydrogen as function of the electron density from the e+OCP model and WPMD simulations at $T=300$ K for 128 and 250 electrons per simulation box.

IV. HYDROGEN EQUATION OF STATE AND CONDUCTIVITY

The isotherms of hydrogen and deuterium at room temperature $T=300$ K have been measured up to a density $n=7\times10^{29}$ m^{-3} with diamond-anvil experiments [1,2]. Even for the largest density the pressure of both isotopes differs by less than 1 GPa, the simulations are therefore done for hydrogen only. Figure 4 shows the isotherms in a semilogarithmic plot. The solid curve is a fit to the experiments, the symbols represent results from fixed-node diffusion Monte Carlo (DMC) simulation [59], DFT calculations [29], as well as WPMD results for 250 electrons per simulation box. The simulation methods yield pressures which are somewhat higher than the experimental values but agree quite well among each other. Up to a density $n=6\times10^{29}$ m^{-3} the present fully antisymmetrized WPMD agrees well with earlier results where the antisymmetrization of the electron-electron interaction was neglected [48,49]. At higher densities a close inspection shows for each method a region in

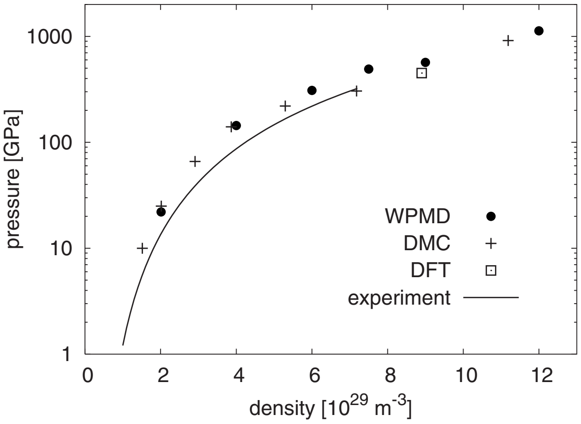

FIG. 4. Pressure as a function of the electron density at $T=300$ K. The solid curve is a fit to the experimental data [1,2], symbols are results from DMC [59] and DFT [29] calculations and WPMD (MC) simulations with 250 electrons per simulation box.

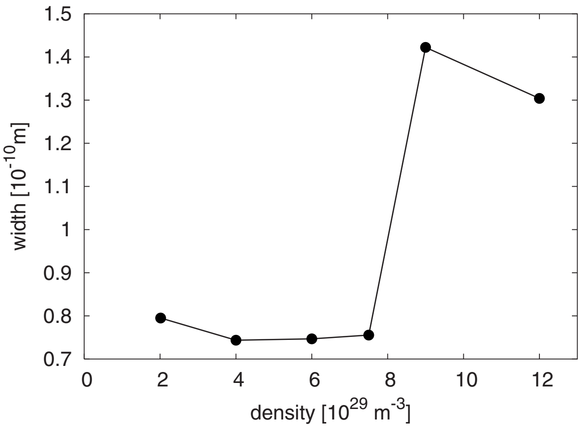

FIG. 5. Mean width of the wave packets as a function of the electron density at $T=300$ K and for 250 electrons per simulation box.

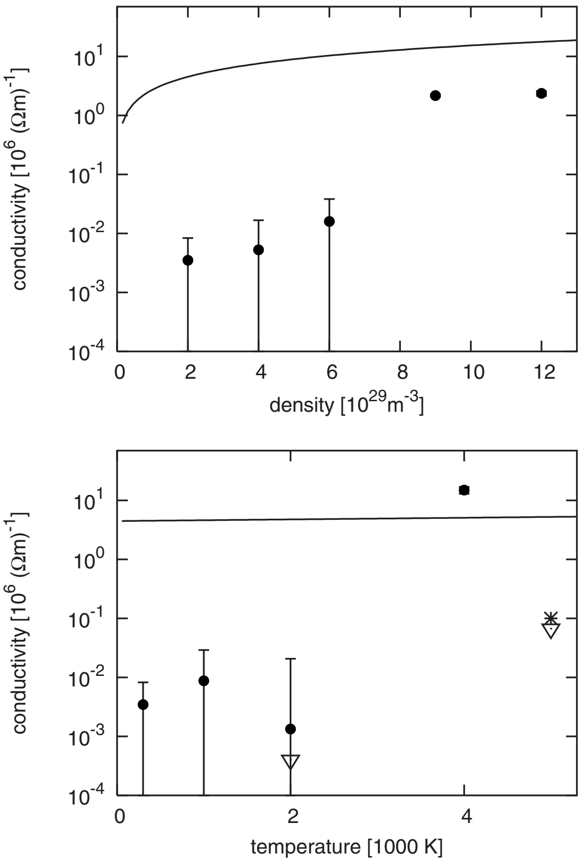

FIG. 6. Upper part: The dc conductivity at $T=300$ K as a function of the density. Lower part: The dc conductivity for $n=2\times10^{29}$ m^{-3} as a function of the temperature. The WPMD results are given by the filled circles with error bars. The number of electrons per simulation box was 250 for the simulations at $T=300$ K and 128 at the larger temperatures. The solid curves show the predictions of an interpolation formula for the conductivity of moderately coupled plasmas [65]. The other symbols in the lower part are the conductivities as obtained in GGA (star) [which vanishes at $T=2000$ K] and TBMD (triangles) calculations along a Hugoniot [64].

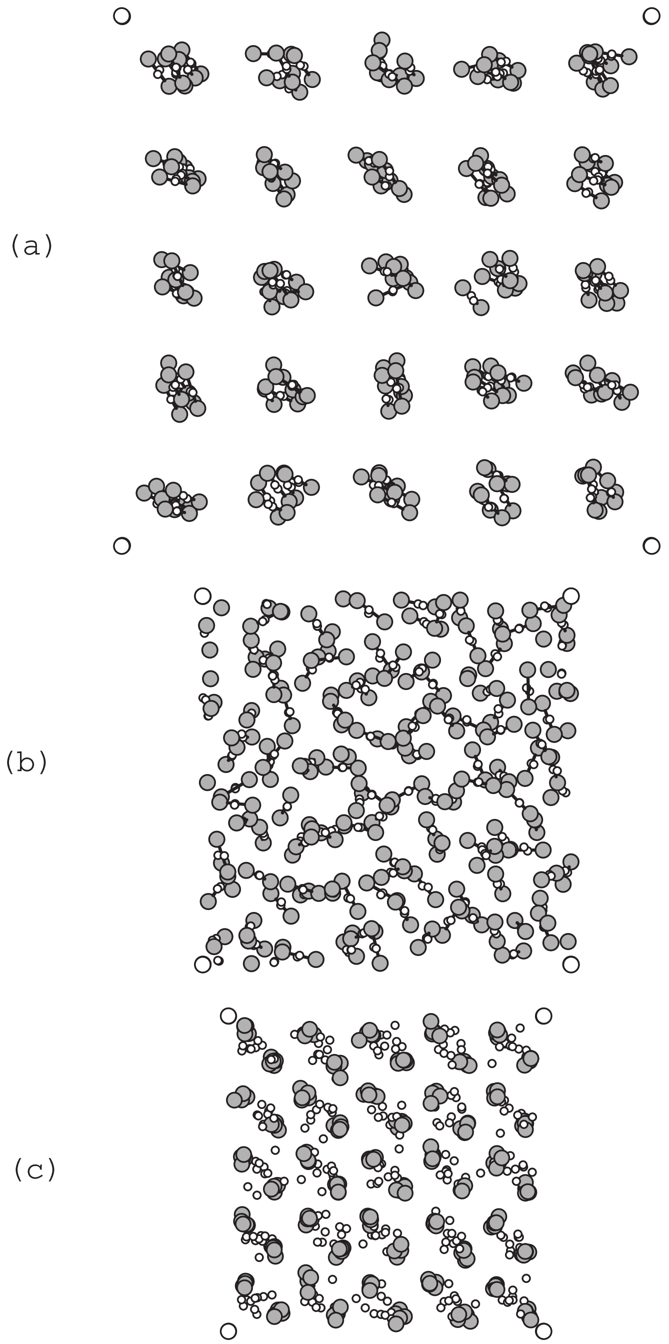

FIG. 7. Projection of the particle coordinates onto one plane of the simulation box. The gray circles are the protons, the small white circles the centers of the electrons, the large white circles mark the size of the simulation box. The results are collected from WPMD simulations with 250 electrons per simulation box at a temperature of $T=300$ K and for three different densities: (a) $n=2\times10^{29}$ m^{-3}, (b) $n=6\times10^{29}$ m^{-3}, (c) $n=9\times10^{29}$ m^{-3}.

which the slope of $P(n)$ levels off. This occurs in the DMC simulations at $n\approx7\times10^{29}$ m^{-3} while the WPMD simulations place this at a higher density near $n=9\times10^{29}$ m^{-3} in agreement with the DFT. The effect is at the edge of visibility in the pressure plot. As supporting information we show in Fig. 5 the average width γ of the wave packets from WPMD simulations. Quite generally one expects that the in-

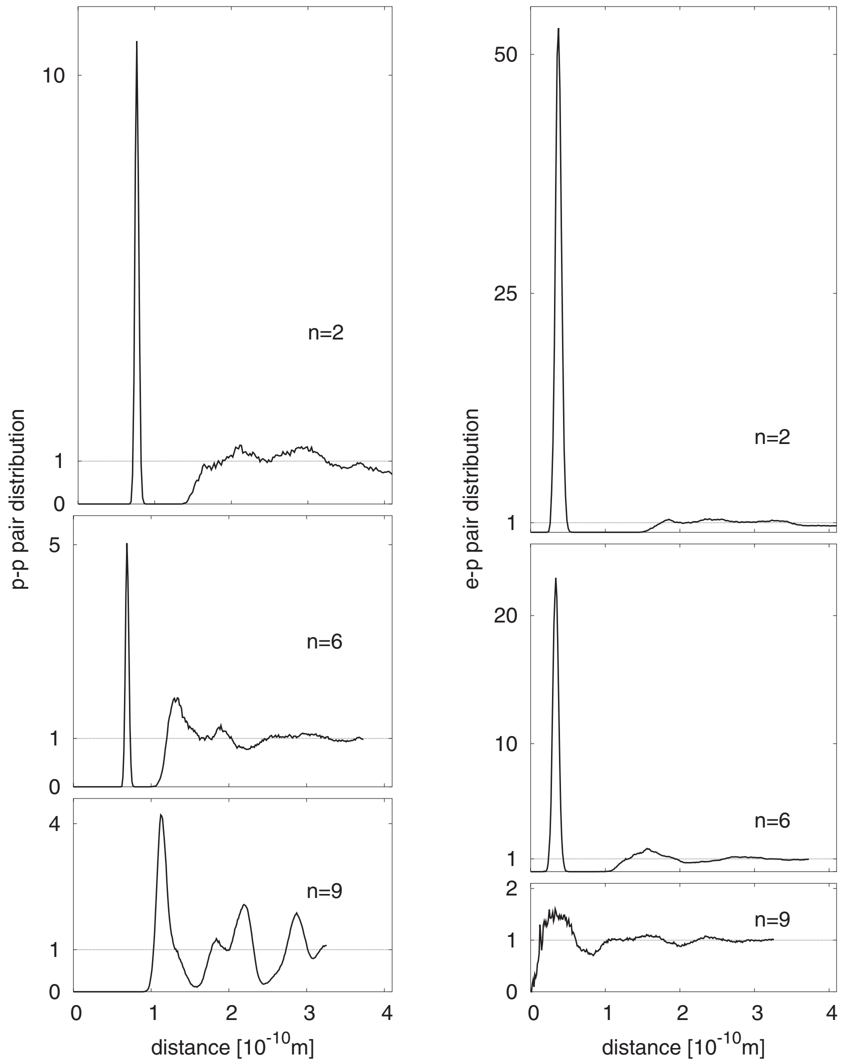

FIG. 8. Proton-proton (left part) and electron-proton (right part) pair distribution from WPMD simulations with 250 electrons per simulation box at $T=300$ K and various densities $n=2\times10^{29}$ m^{-3} (top), $n=6\times10^{29}$ m^{-3} (center), $n=9\times10^{29}$ m^{-3} (bottom).

teractions influence the spatial extension of the wave packets from the de Broglie wavelength at weak coupling to the Bohr radius typical for bound states at strong coupling, i.e., for large densities and low temperatures. This behavior is, e.g., reflected in the softening of effective pair potentials [44,45,60,61]. Here the width of the wave packets does not vary smoothly, but jumps by a factor of 2 at the critical density. We interpret this as a transition from a molecular state with localized electrons to a metallic state with extended electron clouds.

As further support for that interpretation, we have calculated the conductivity σ with the help of a dynamic simulation (6) of the current-current autocorrelation function [62]

$$\sigma(\tau) = \frac{\beta}{3L^3}\int_0^\tau dt\langle\vec{j}(t)\cdot\vec{j}(0)\rangle$$

$$= \frac{\beta}{3L^3}\int_0^\tau dt\frac{1}{T}\int_0^T dt'\vec{j}(t'+t)\cdot\vec{j}(t'). \qquad (31)$$

The dc conductivity is obtained in the limit $\tau\rightarrow\infty$. The simulation runs only for a limited time interval $[0,T_{\text{sim}}]$ and thus the autocorrelation function can be evaluated only for a time interval $[0,T_{\text{sim}}-t]$. It shrinks with increasing analyzing time t which, in turn, enhances the statistical fluctuations for $t\rightarrow T_{\text{sim}}$. As the current is mainly carried by the electrons, we simulate for 100 electronic plasma periods to obtain an estimate for σ. Because of the fluctuating integrand the convergence is extremely poor in the transition region and the conductivities in the molecular regime should be regarded as upper limits. In practice, they are probably even lower. In spite of the limitations of the analysis, the results in Fig. 6 show nicely an increase of the conductivity by orders of magnitude: at a critical density of $n=9\times10^{29}$ m^{-3} along the isotherm (upper part) and similarly at a temperature of $T\approx3000-4000$ K for an isochoric change at fixed $n=2\times10^{29}$ m^{-3} (lower part). These jumps in conductivity indicate a typical insulator-metal transition. In the lower part of Fig. 6 results are shown which where obtained in GGA and TBMD calculations along a Hugoniot [64]. They indicate a smaller jump in the conductivity between 2000 and 5000 K for $n=2\times10^{29}$ m^{-3}. The solid curves in Figs. 6 represent the electric conductivity of moderately coupled, fully ionized plasmas as provided by the interpolation formula from Ref. [65]. (The limiting Spitzer formula [63] is not applicable here because of the strong coupling.) These curves serve here

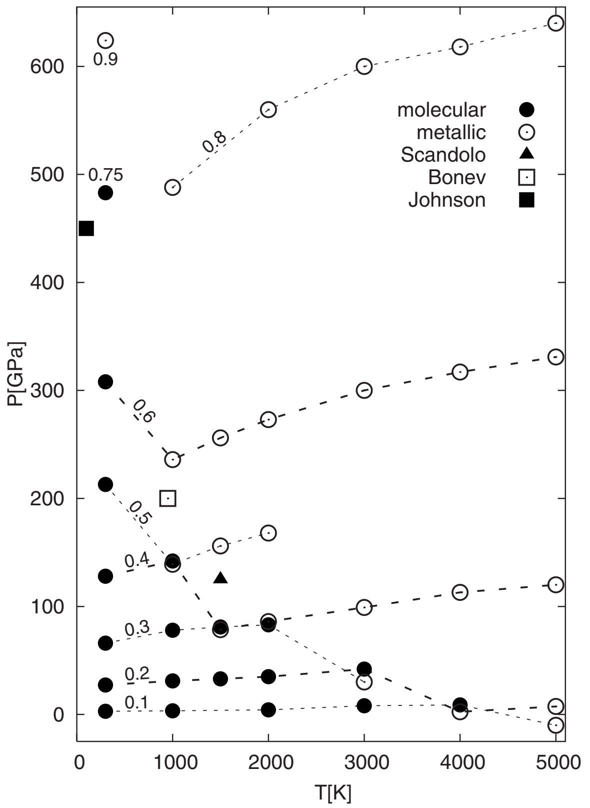

FIG. 9. Phase diagram of dense hydrogen as obtained by WPMD calculations. Filled circles signify the molecular phase and open circles the metallic phase. States of equal density are connected by lines and labeled by the value of the density in units of 10^{30} m^{-3}. The number of electrons per simulation box was 250 at $T=300$ K and 128 at the higher temperatures. The other symbols show points at the phase transition as obtained from density functional calculations [29,33,34].

as reference for the typical values of the conductivity of a fully ionized plasmas, where nonideality effects are already taken into account. For more sophisticated theoretical treatments of the conductivity which also consider the influence of bound states, as essential in the present parameter regimes, see, e.g., Ref. [66]. Our result at $T=4000$ K lies above the interpolation curve given in the lower part of Fig. 6. In this temperature regime the Gaussian wave packets (11b) may not be sufficiently flexible to describe the electron-ion scattering correctly. We will return to this problem below. Increasing conductivities have been observed in measurements at constant Hugoniot. Earlier shock experiments involving temperatures between 3000 and 4500 K show an increase from $\sigma \approx 3\times 10^{-3}$ $(\Omega\ \mathrm{m})^{-1}$ to $\sigma \approx 50$ $(\Omega\ \mathrm{m})^{-1}$ [67]. An interpolation with later multiple shock experiments [68] yields a jump from $\sigma \approx 3\times 10^{-3}$ $(\Omega\ \mathrm{m})^{-1}$ to $\sigma \approx 2\times 10^{5}$ $(\Omega\ \mathrm{m})^{-1}$ at 3000 K [69]. The transition can also be visualized in terms of the spatial distributions of the particles. To that end, we project the particle coordinates into one plane of the simulation box. The results are shown in Fig. 7. Figure 7(a) for $n=2\times 10^{29}$ m^{-3} shows a molecular bcc crystal with the electrons localized between the two protons of the H_2 molecules. Around $n=6\times 10^{29}$ m^{-3}, Fig. 7(b), the crystal begins to dissolve forming a molecular fluid, this stage requires extremely long simulation times. Melting has been observed at much lower pressures (≈ 6 GPa) and densities in refraction experiments [70], while the experiments on the isotherm at room temperature [1] shown in Fig. 4 remain in the solid regime. At $n=9\times 10^{29}$ m^{-3}, Fig. 7(c), the protons form a cubic fcc grid, and because of their large width the electrons can move freely between the sites. These values of density and temperature lie within a predicted stability region for two-component Coulomb crystals [71].

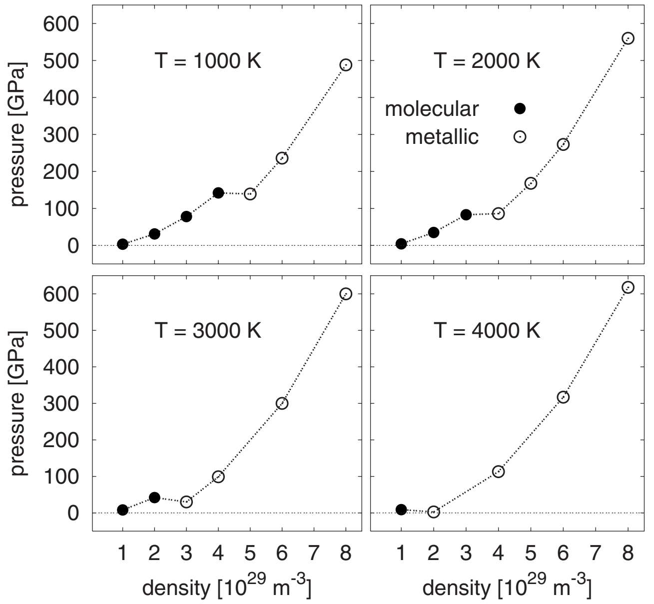

FIG. 10. Pressure of dense hydrogen as a function of the electron density at various temperatures $T=1000\ldots5000$ K. As in Fig. 9, filled circles indicate the molecular phase and open circles the metallic phase, respectively. The number of electrons per simulation box was 128 for all shown settings.

A more compact and quantitative view of the system's structure is provided by the pair distribution functions, the cumulated probability to find two particles at a given distance. It is sampled in practice in radial bins. The large number of particles and MC samples allows a rather fine binning yielding a nicely smooth looking curve. The left part of Fig. 8 shows the proton-proton pair distribution function for the three cases discussed above. The change in structure with changing density is clearly seen. At $n=2\times 10^{29}$ m^{-3} the strong nearest-neighbor peak agrees well with the bond length 0.8×10^{-10} m of the protons in the free H_2 molecule. The long-range order is washed out because of thermal vibration and molecular rotation. At the next higher density, this structure disappears as one passes through a molecular fluid phase. Further increase in density to $n=9\times 10^{29}$ m^{-3} produces new structures which now are caused by the long-range correlation of the cubic fcc lattice of protons immersed in a practically homogeneous electron gas. The electron-proton pair distribution functions in the right part of Fig. 8 show for $n=2\times 10^{29}$ m^{-3} a peak near 0.4×10^{-10} m, i.e., the electrons are concentrated between two protons which form the H_2 molecule. With increasing density the molecules

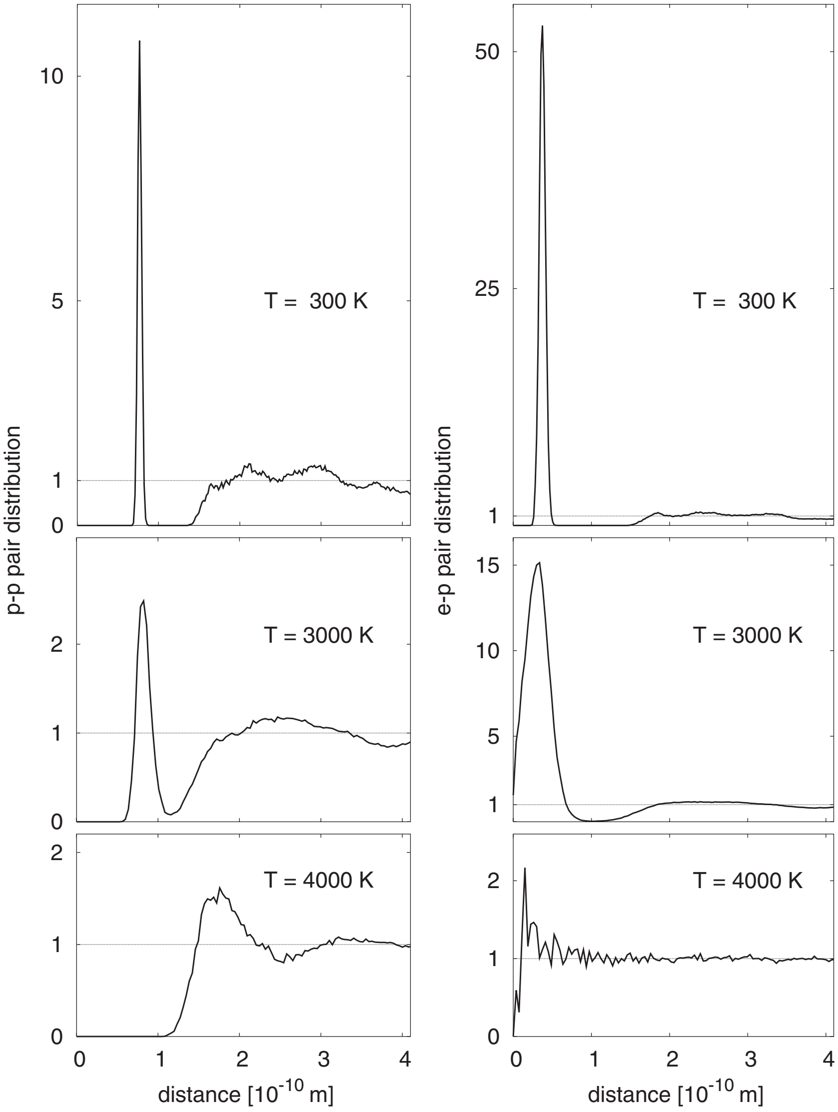

FIG. 11. Proton-proton (left part) and electron-proton (right part) pair distribution from WPMD simulations at $n=2\times10^{29}\ \mathrm{m}^{-3}$ and different temperatures $T=300$ K, $T=3000$ K, and $T=4000$ K.

disappear and the pair distribution function becomes flatter. But there is no enhancement near zero distance, which indicates that there are no atoms.

Up to here, we have reported in detail results for $T=300$ K and various densities. We have performed WPMD calculations of dense hydrogen within a broad range of conditions, for electron densities $n=(1-9)\times10^{29}\ \mathrm{m}^{-3}$ and temperatures up to $T=5000$ K. The results are summarized in Fig. 9 in terms of a phase diagram in the T-P plane. The filled symbols indicate the molecular phase and the open symbols the metallic phase. There is a clear separation of the two regimes associating low T and P to the molecular stage. Phase coexistence can be found at the border between the two regimes. Both phases can occur at the same values of temperature and pressure, but with different density, the metallic phase being denser than the molecular one. In a large system, both phases should segregate and drops, or even an extended phase boundary should form. This is not yet observed in the present simulations. The particle number of 250 electrons per simulation box is still too small. Density functional calculations at selected points in the T-P plane also yield the phase transition from a molecular to a metallic phase associated by an increase in density [29,33,34]. Their results are shown in Fig. 9 for comparison. They lie well on the separation curve emerging from our simulations. In Fig. 10 we show isotherms in the n-P plane which demonstrate a first-order phase transition from the molecular to the metallic state. Experimental evidence for such a transition in this range of densities, temperatures, and pressures has recently been obtained by a quasi-isentropic compression of a deuterium plasma in reverberating shock wave experiments [72]. It is also interesting to note that the coexistence region which can be deduced from Figs. 9 and 10 resembles very much the bananalike domain of a first order insulator-to-metal transition as shown in Fig. 1 of Ref. [73]. There the transition occurs at a density of about $5.5\times10^{29}\ \mathrm{m}^{-3}$ for temperatures below 2000 K. At higher temperatures the coexistence region turns toward much lower densities and ends at a critical point near $T\approx40\,000$ K and $n\approx2\times10^{26}\ \mathrm{m}^{-3}$.

Additional information about the changes in the system at increasing temperature can be obtained again from the pair distribution functions. In Fig. 11 we plotted the proton-proton (left part) and the electron-proton (right part) pair distribution functions for different temperatures at a density

$n=2\times10^{29}$ m^{-3}. As in the case of increasing density at constant $T=300$ K (Fig. 8) the change from a molecular system to a metallic fluid, where the protons are embedded in an almost homogeneous electron gas, is again clearly visible. In contrast to the strongly correlated proton crystal seen at $n=9\times10^{29}$ m^{-3} and $T=300$ K (Fig. 8, left bottom), the proton-proton pair distribution function at $T=4000$ K and $n=2\times10^{29}$ m^{-3} (Fig. 11, left bottom) now shows a moderately coupled proton OCP. The enhancement in the electron-proton pair distribution near zero distance at $T=3000$ K (Fig. 11, right center) here indicates the existence of a small fraction of atoms or atomlike configurations during the change from the molecular state at $T=300$ K to the practically free electron gas at $T=4000$ K.

V. SUMMARY AND CONCLUSIONS

We have extended previous formulations of the WPMD by implementing full antisymmetrization for the electron-electron interaction and by introducing approximate Bloch waves in order to account for the periodic continuation of the simulation box. The basis states (11a) and (11b) are not orthogonal which leads for properly antisymmetrized many-body wave functions to a modified volume element in the MC sampling (10a) and (10b) [without antisymmetrization and for Gaussian wave packets (11b) this volume element happens to be 1]. The overlap of the wave packets increases with the width of the wave packets. The complete antisymmetrization of the many-body wave function for all terms of the expectation values of the Hamiltonian prevents an unphysical growth of the width by virtue of the presence of the modified volume element (10a) and (10b). There is no more need for introducing an *ad hoc* external potential as in previous WPMD simulations [48,49,54].

We have used the extended scheme to perform WPMD simulations for dense hydrogen. As a benchmark, we have compared the results with experiments and competing models. The equation of state at $T=300$ K agrees well with diffusion Monte Carlo results. Both theoretical curves yield somewhat higher pressures than observed in the diamond-anvil experiments, which were carried out up to densities $n=7\times10^{29}$ m^{-3}. The simulation results show a transition from molecular hydrogen to a metallic phase with delocalized electrons. The transition was analyzed and confirmed by examining several observables, trend in pressure, spatial widths of electronic wave functions, conductivity, particle distributions, and pair-distribution functions. The experimental results stop presently somewhat lower than the predicted transition point near $n=9\times10^{29}$ m^{-3}.

Systematic simulations for a wide range of densities and temperatures yield a clear transition curve in the T-P plane with a molecular phase at low temperatures and/or pressures and a metallic state otherwise. Results from density functional calculations lie very close to the results from WPMD. At the transition curve, there is a regime of phase transition where metallic and molecular phases can coexist at the same temperature and pressure, however, at much different densities (metallic hydrogen having larger density than molecular hydrogen).

It is desirable to extend the simulations to dense hydrogen at higher temperatures $T\geq5000$ K, as they occur in the shock wave experiments [4–10,67,68]. At these higher temperatures the present Gaussian ansatz (11b) for the wave packets seems not to be sufficient [55]. Electron scattering at higher momenta becomes important there and preliminary studies have shown that this regime requires an extension of the wave packets to allow for two different length scales in one electronic wave function which, in turn, requires more variational parameters [74,75]. Moreover electron-electron correlations beyond ensembles of Slater determinants constructed from wave packets (11a) and (11b) could be included in the framework of the unitary correlator method [76]. This is a task for future development.

ACKNOWLEDGMENTS

This work has been supported by the BMBF, the Gesellschaft für Schwerionenforschung (GSI), and the John von Neumann Institute for Computing in Jülich.

---

[1] P. Loubeyre, R. LeToullec, D. Hausermann, M. Hanfland, R. J. Hemley, H. K. Mao, and L. W. Finger, Nature (London) **383**, 702 (1996).

[2] P. Loubeyre, F. Occelli, and R. LeToullec, Nature (London) **416**, 613 (2002).

[3] W. J. Nellis, S. T. Weir, and A. C. Mitchell, Phys. Rev. B **59**, 3434 (1999).

[4] L. B. Da Silva, P. Celliers, G. W. Collins, K. S. Budil, N. C. Holmes, T. W. Barbee, Jr., B. A. Hammel, J. D. Kilkenny, R. J. Wallace, M. Ross, R. Cauble, A. Ng, and G. Chiu, Phys. Rev. Lett. **78**, 483 (1997).

[5] G. W. Collins, P. Celliers, L. B. Da Silva, R. Cauble, D. Gold, M. Ford, K. S. Budil, R. Stewart, N. C. Holmes, M. Ross, B. A. Hammel, J. D. Kilkenny, R. J. Wallace, and A. Ng, Phys. Plasmas **5**, 1864 (1998).

[6] M. D. Knudson, D. L. Hanson, J. E. Bailey, C. A. Hall, J. R. Asay, and W. W. Anderson, Phys. Rev. Lett. **87**, 225501 (2001).

[7] M. D. Knudson, D. L. Hanson, J. E. Bailey, C. A. Hall, and J. R. Asay, Phys. Rev. Lett. **90**, 035505 (2003).

[8] M. D. Knudson, D. L. Hanson, J. E. Bailey, C. A. Hall, J. R. Asay, and C. Deeney, Phys. Rev. B **69**, 144209 (2004).

[9] S. I. Belov, G. V. Boriskov, A. I. Bykov, R. I. Ilkaev, N. B. Lukyanov, A. Ya. Matveev, O. L. Mikhailova, V. D. Selemir, G. V. Simalov, R. F. Trunin, I. P. Trusov, V. D. Urlin, V. E. Fortov, and A. N. Shuikin, JETP Lett. **76**, 433 (2002).

[10] G. V. Boriskov, A. I. Bykov, R. I. Ilkaev, V. D. Selemir, G. V. Simakov, R. F. Trunin, V. D. Urlin, A. N. Shuikin, and W. J. Nellis, Phys. Rev. B **71**, 092104 (2005).

[11] G. Chabrier, D. Saumon, W. B. Hubbard, and J. I. Lunine,

Astrophys. J. **391**, 817 (1992).

[12] D. Saumon, W. B. Hubbard, G. Chabrier, and H. M. Van Horn, Astrophys. J. **391**, 827 (1992).

[13] R. Redmer, B. Holst, H. Juranek, N. Nettelmann, and V. Schwarz, J. Phys. A **39**, 4479 (2006).

[14] J. Vorberger, I. Tamblyn, B. Militzer, and S. A. Bonev, Phys. Rev. B **75**, 024206 (2007).

[15] M. P. Desjarlais, Phys. Rev. B **68**, 064204 (2003).

[16] J. Lindl, Phys. Plasmas **2**, 3933 (1995).

[17] G. R. Bennett, M. E. Cuneo, R. A. Vesey, J. L. Porter, R. G. Adams, R. A. Aragon, J. A. Caird, O. L. Landen, P. K. Rambo, D. C. Rovang, L. E. Ruggles, W. W. Simpson, I. C. Smith, and D. F. Wenger, Phys. Rev. Lett. **89**, 245002 (2002).

[18] E. Wigner and H. B. Huntington, J. Chem. Phys. **3**, 764 (1935).

[19] W. Ebeling, W. D. Kraeft, and D. Kremp, *Theory of Bound States and Ionization Equilibrium in Plasmas and Solid* (Akademie Verlag, Berlin, 1976).

[20] W. D. Kraeft, D. Kremp, W. Ebeling, and G. Röpke, *Quantum Statistics of Charged Particle Systems* (Akademie Verlag, Berlin, 1986).

[21] M. Ross, Phys. Rev. B **58**, 669 (1998).

[22] D. Saumon and G. Chabrier, Phys. Rev. A **46**, 2084 (1992).

[23] H. Juranek, R. Redmer, and Y. Rosenfeld, J. Chem. Phys. **117**, 1768 (2002).

[24] T. J. Lenosky, J. D. Kress, L. A. Collins, R. Redmer, and H. Juranek, Phys. Rev. E **60**, 1665 (1999).

[25] L. Collins, I. Kwon, J. Kress, N. Troullier, and D. Lynch, Phys. Rev. E **52**, 6202 (1995).

[26] R. Car and M. Parrinello, Phys. Rev. Lett. **55**, 2471 (1985).

[27] D. Hohl, V. Natoli, D. M. Ceperley, and R. M. Martin, Phys. Rev. Lett. **71**, 541 (1993).

[28] J. Kohanoff and J.-P. Hansen, Phys. Rev. E **54**, 768 (1996).

[29] K. A. Johnson and N. W. Ashcroft, Nature (London) **403**, 632 (2000).

[30] T. J. Lenosky, S. R. Bickham, J. D. Kress, and L. A. Collins, Phys. Rev. B **61**, 1 (2000).

[31] G. Galli, R. Q. Hood, A. U. Hazi, and F. Gygi, Phys. Rev. B **61**, 909 (2000).

[32] B. Militzer, D. M. Ceperley, J. D. Kress, J. D. Johnson, L. A. Collins, and S. Mazevet, Phys. Rev. Lett. **87**, 275502 (2001).

[33] S. Scandolo, Proc. Natl. Acad. Sci. U.S.A. **100**, 3051 (2003).

[34] S. A. Bonev, E. Schwegler, T. Ogitsu, and G. Galli, Nature (London) **431**, 669 (2004).

[35] B. Militzer and E. L. Pollock, Phys. Rev. E **61**, 3470 (2000).

[36] W. R. Magro, D. M. Ceperley, C. Pierleoni, and B. Bernu, Phys. Rev. Lett. **76**, 1240 (1996).

[37] B. Militzer and D. M. Ceperley, Phys. Rev. Lett. **85**, 1890 (2000).

[38] V. S. Filinov, M. Bonitz, W. Ebeling, and V. E. Fortov, Plasma Phys. Controlled Fusion **43**, 743 (2001).

[39] V. S. Filinov, M. Bonitz, V. E. Fortov, W. Ebeling, P. R. Levashov, and M. Schlanges, Contrib. Plasma Phys. **44**, 388 (2004).

[40] V. Bezkrovniy, V. S. Filinov, D. Kremp, M. Bonitz, M. Schlanges, W. D. Kraeft, P. R. Levashov, and V. E. Fortov, Phys. Rev. E **70**, 057401 (2004).

[41] E. J. Heller, J. Chem. Phys. **62**, 1544 (1975).

[42] H. Feldmeier, Nucl. Phys. A. **515**, 147 (1990).

[43] H. Feldmeier and J. Schnack, Rev. Mod. Phys. **72**, 655 (2000).

[44] D. Klakow, C. Toepffer, and P.-G. Reinhard, J. Chem. Phys. **101**, 10766 (1994).

[45] D. Klakow, C. Toepffer, and P.-G. Reinhard, Phys. Lett. A **192**, 55 (1994).

[46] S. Nagel, R. Redmer, G. Röpke, M. Knaup, and C. Toepffer, Phys. Rev. E **57**, 5572 (1998).

[47] M. Knaup, P.-G. Reinhard, and C. Toepffer, Contrib. Plasma Phys. **39**, 57 (1999).

[48] M. Knaup, G. Zwicknagel, P.-G. Reinhard, and C. Toepffer, Nucl. Instrum. Methods Phys. Res. A **464**, 267 (2001).

[49] M. Knaup, P.-G. Reinhard, C. Toepffer, and G. Zwicknagel, J. Phys. A **36**, 6165 (2003).

[50] M. P. Allen and D. J. Tildesley, *Computer Simulations of Liquids* (Clarendon Press, Oxford, 1987), Chaps. 2,4,5.

[51] A. L. Fetter and J. D. Walecka, *Quantum Theory of Many-Particle Sytems* (McGraw-Hill, New York, 1971), Chap. 3, p. 4.

[52] P. P. Ewald, Ann. Phys. **64**, 253 (1921).

[53] W. H. Press, S. A. Teukolsky, W. T. Vetterling, and B. P. Flannery, *Numerical Recipes in C* (Cambridge University Press, Cambridge, 1992), Chap. 16.

[54] M. Knaup, *Die Methode der Wellenpakets-Molekulardynamik (WPMD) mit Anwendungen auf Wasserstoff* (Shaker Verlag, Aachen, 2002).

[55] B. Jakob, Ph.D. thesis, Universität Erlangen, Erlangen, 2006. (http://www.opus.ub.uni-erlangen.de/opus/volltexte/2006/469/).

[56] L. D. Landau and E. M. Lifshitz, *Statistical Physics* (Pergamon Press, London, 1959), Chap. 31.

[57] See, for example, S. Ichimaru, *Statistical Plasma Physics* (Addison-Wesley, Reading, 1994), Vol. 2, Chap. 2.

[58] H. E. DeWitt and W. L. Slattery, in *Strongly Coupled Coulomb Systems*, edited by G. J. Kalman, J. M. Rommel, and K. Blagoev (Plenum Press, New York, 1998), p. 1.

[59] D. M. Ceperley and B. J. Alder, Phys. Rev. B **36**, 2092 (1987).

[60] A. V. Filinov, V. O. Golubnychiy, M. Bonitz, W. Ebeling, and J. W. Dufty, Phys. Rev. E **70**, 046411 (2004).

[61] W. Ebeling, A. Filinov, M. Bonitz, V. Filinov, and T. Pohl, J. Phys. A **39**, 4309 (2006).

[62] See, for example, D. M. Zubarev, V. Morozov, and G. Röpke, *Statistical Mechanics of Nonequilibrium Processes* (Akademie Verlag, Berlin, 1997), Vol. 2, Chap. 5.1.7.

[63] L. Spitzer and R. Härm, Phys. Rev. **89**, 977 (1953).

[64] L. A. Collins, S. R. Bickham, J. D. Kress, S. Mazevet, T. J. Lenosky, N. J. Troullier, and W. Windl, Phys. Rev. B **63**, 184110 (2001).

[65] A. Esser, R. Redmer, and G. Röpke, Contrib. Plasma Phys. **43**, 33 (2003).

[66] R. Redmer, G. Röpke, S. Kuhlbrodt, and H. Reinholz, Phys. Rev. B **63**, 233104 (2001).

[67] W. J. Nellis, A. C. Mitchell, P. C. McCandless, D. J. Erskine, and S. T. Weir, Phys. Rev. Lett. **68**, 2937 (1992).

[68] S. T. Weir, A. C. Mitchell, and W. J. Nellis, Phys. Rev. Lett. **76**, 1860 (1996).

[69] A. Bunker, S. Nagel, R. Redmer, and G. Röpke, in *Strongly Coupled Coulomb Systems*, edited by G. J. Kalman, J. M. Rommel, and K. Blagoev (Plenum Press, New York, 1998), p. 365.

[70] F. Datchi, P. Loubeyre, and R. LeToullec, Phys. Rev. B **61**, 6535 (2000).

[71] M. Bonitz, V. S. Filinov, V. E. Fortov, P. R. Levashov, and H. Fehske, Phys. Rev. Lett. **95**, 235006 (2005).

[72] V. E. Fortov, R. I. Ilkaev, V. A. Arinin, V. V. Burtzev, V. A. Golubev, I. L. Iosilevskiy, V. V. Khrustalev, A. L. Mikhailov, M. A. Mochalov, V. Y. Ternovoi, and M. V. Zhernokletov, Phys. Rev. Lett. (to be published).

[73] H. Kitamura and S. Ichimaru, J. Phys. Soc. Jpn. **67**, 950 (1998).

[74] J. Marten, Ph.D. thesis, Universität Erlangen, Erlangen, 1998.

[75] A. Lenglet and G. Maynard, Nucl. Instrum. Methods Phys. Res. A **577**, 343 (2007).

[76] H. Feldmeier, T. Neff, R. Roth, and J. Schnack, Nucl. Phys. A **632**, 61 (1998).